Proceedings of ALGORITMY 2009
pp. 61–70

NEW LIMITER FUNCTIONS FOR HIGH-ORDER FINITE-VOLUME-METHODS

MIROSLAV ČADA* AND MANUEL TORRILHON †

Abstract. We consider finite volume methods for the numerical solution of conservation laws. In order to achieve high-order accurate numerical approximation to nonlinear smooth functions, we introduce a new class of nonlinear and non-polynomial limiter functions for the spatial reconstruction of hyperbolic equations. The new scheme is of third-order accuracy. Its shape preserving properties are significantly improved. Discontinuities are reconstructed sharp and accurate. Smearing, clipping and squaring effects of classical second-order limiters are completely avoided.

Key words. Finite-Volume-methods, limiters, high-order accuracy, shock-capturing, logarithmic limiter.

AMS subject classifications. 15A15, 15A09, 15A23

1. Introduction. In the present paper we will derive a new third-order accurate method for the computation of numerical fluxes within the framework of finite volume (FV) schemes for conservation laws. For simplicity and in order to settle our notation we consider the numerical approximations to the one-dimensional scalar initial value problem

$$u_t = -f(u)_x, \quad \text{with} \quad u(x, t=0) = u_0(x), \tag{1}$$

where u_0 is either a piecewise smooth function with compact support or a periodic function. Note that the flux in Eq. (1) appears on the right hand side to emphasize the semi-discrete formulation. We cover the uniform computational region with control cells $C_i^n = [x_{i-\Delta x/2}, x_{i+\Delta x/2}] \times [t^n, t^{n+1}]$, with $t^{n+1} = t^n + \Delta t$ and the computational grid $x_{i\pm1} = x_i \pm \Delta x$. Integrating the conservation law Eq. (1) over the control volume C_i, we obtain the standard FV update

$$\begin{aligned} \frac{d}{dt}\bar{u}_i &= L_i(\bar{u}^n) \\ &= \frac{1}{\Delta x}\big[\mathcal{F}(\hat{u}^{(-)}_{i-\frac{1}{2}}, \hat{u}^{(+)}_{i-\frac{1}{2}}) - \mathcal{F}(\hat{u}^{(-)}_{i+\frac{1}{2}}, \hat{u}^{(+)}_{i+\frac{1}{2}})\big], \end{aligned} \tag{2}$$

for the cell average $\bar{u}_i^n = \frac{1}{\Delta x}\int_{x_{i-\Delta x/2}}^{x_{i+\Delta x/2}} u^n(x)\,\mathrm{dx}$ at time t^n based on the numerical flux function $\mathcal{F}$, which is supposed to be Lipschitz continuous and consistent with the flux $f(u)$. The evolution of $\bar{u}_i^n$ is governed by the left and right limits $\hat{u}^{(\pm)}_{i+\frac{1}{2}}$ – the interface values – of the reconstructed function $\hat{u}(x)$. The cell interface value $\hat{u}_{i+\frac{1}{2}} = \hat{u}(\bar{u}_i^n, \bar{u}_{i+1}^n)$ denotes the intermediate value at $x_{i+1/2}$ of the Riemann problem solution with initial data $\bar{u}_i^n, \bar{u}_{i+1}^n$. *The calculation of the interface values from the known cell mean values is the essential reconstruction task and determines the scheme's order of accuracy.* This is the main concern of this paper.

*Seminar for Applied Mathematics, ETH-Zurich, Switzerland, (cada@math.ethz.ch).
†Seminar for Applied Mathematics, ETH-Zurich, Switzerland, (mattoril@math.ethz.ch).

2. Compact Finite Volume Reconstruction based upon Limiters. In this section we review spatial reconstruction techniques, which adopt a local three-point stencil and are related to limiter functions. Hence the interface values are functions of nearest neighbours, i.e $\hat{u}^{(-)}_{i+\frac{1}{2}} \equiv L(\bar{u}_{i-1}, \bar{u}_i, \bar{u}_{i+1})$ and $\hat{u}^{(+)}_{i+\frac{1}{2}} \equiv R(\bar{u}_i, \bar{u}_{i+1}, \bar{u}_{i+2})$, where capital L and capital R denote the left and right cell interface approximations, respectively. In order to obtain high order non-oscillatory reconstructions, the interpolation function R and L are a priori nonlinear.

We assume, that the cell-face values are calculated with an upwind-biased approach, i.e.

$$\hat{u}^{(-)}_{i+\frac{1}{2}} = \bar{u}_i + \frac{1}{2}\phi(\theta_i)\,\delta_{i+\frac{1}{2}} \qquad (3)$$
$$\hat{u}^{(+)}_{i-\frac{1}{2}} = \bar{u}_i - \frac{1}{2}\phi(\theta_i^{-1})\,\delta_{i-\frac{1}{2}}$$

where $\delta_{i+\frac{1}{2}} = \bar{u}_{i+1} - \bar{u}_i$ is the difference across a cell interface, and $\phi(\theta_i)$ is the limiter with

$$\theta_i = \frac{\delta_{i-\frac{1}{2}}}{\delta_{i+\frac{1}{2}}}, \quad \text{with} \quad \delta_{i+\frac{1}{2}} \neq 0 \qquad (4)$$

is a local smoothness measurement. It can be clearly seen that the reconstruction Eqs. (3) employ a rather simple Taylor expansion. Yet to approximate the cell interface values Eqs. (3) to third-order accuracy, the first derivatives at $x_{i\pm 1/2}$ have to be of second order accuracy, i.e $u'(x_{i\pm\frac{1}{2}}) = \delta_{i\pm\frac{1}{2}}/\Delta x \pm \mathcal{O}(\Delta x^2)$. Note that in the context of finite-differences, i.e. point value based reconstruction u_i^n and not cell averages based $\bar{u}_i^n$, it holds $u'(x_{i\pm 1/2}) = \delta_{i\pm\frac{1}{2}}/\Delta x \pm \mathcal{O}(\Delta x)$. Thus we recover one order less than employing FV methods. The limiter is defined as a function of consecutive gradients (slopes), i.e. $\phi_i = \phi(\theta_i)$. To avoid spurious oscillations for high order interpolation around discontinuous data, Harten [4] derived explicit algebraic conditions on the limiter ϕ:

$$0 \leq \phi(\theta) \leq 2\,\theta \quad \text{and} \quad 0 \leq \phi(\theta) \leq 2 \quad \forall \theta \geq 0. \qquad (5)$$

Harten's fundamental theorem ensures the resulting scheme to be total variation diminishing (TVD) and hence with an appropriate time integrator to be monotonicity-preserving. The region, which is spanned by Harten's TVD conditions Eqs. (5) is called Sweby's TVD region [6]. Limiter function inside this region are TVD and of high-order accuracy essentially away from smooth extrema and discontinuous data. A major drawback of high-order TVD schemes is their inability to recover smooth extrema. A complete summary of the theory of TVD methods and classical second-order accurate limiters can be found in standard text books, e.g. LeVeque [7].

We should mention that the most well known limiters are of second-order spatial accuracy and satisfy the symmetry condition $\phi(\theta^{-1})\,\theta = \phi(\theta)$. Therefore Eqs. (3) can be simplified and no limiter evaluation of θ^{-1} is necessary. This reduces the amount of floating point operation and makes symmetric second-order limiters quite effective. A necessary condition for limiting methods to be of high-order accuracy, is that the function ϕ must pass Lipschitz continuously through the point $\phi(1) = 1$. There exists a whole set of linear methods, which depend on $\phi'(1)$ and approximate the cell-face

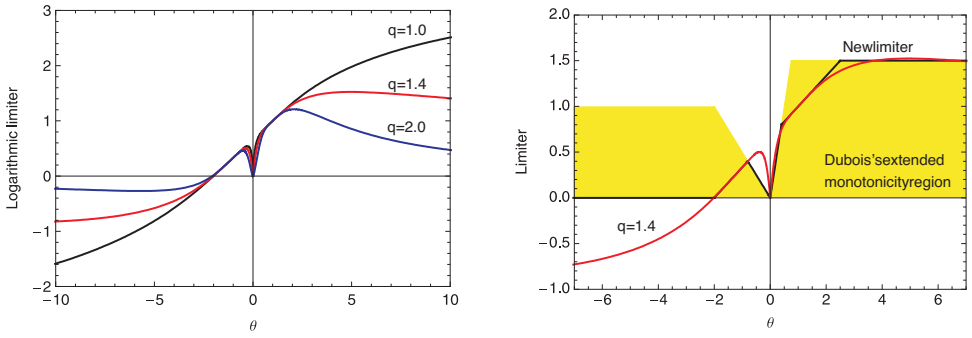

FIG. 1. *Left: Shape of the limiter function $\phi(\theta)$ Eq. (7) for different values of q. Right: New limiter $\hat{\phi}$ Eq. (9) matching for logarithmic limiter with $q = 1.4$.*

values $\hat{u}^{(\mp)}_{i\pm\frac{1}{2}}$ employing Eqs. (3) to second-order accuracy. Yet one finds only one unique reconstruction

$$\phi(\theta) = \frac{2+\theta}{3}, \tag{6}$$

for which we get third-order of spatial accuracy. This function is a parabola through the discrete set of cell mean values $\{\bar{u}_{i-1}, \bar{u}_i, \bar{u}_{i+1}\}$.

3. Logarithmic Limiter. Recently Čada and Torrilhon [5] have derived a new smooth limiter, which applies a logarithmic function as building block. The limiter function is based upon nonlinear and especially non-polynomial local double logarithmic reconstruction (LDLR) suggested by Artebrant and Schroll [1]. The LDLR is essentially of third-order accuracy away from discontinuities without the explicit use of limiters. Due to the logarithmic nature its total variation bound (TVB), in the presence of jump discontinuities, is $\mathcal{O}(\Delta x^q \,|\ln(\Delta x)|)$. It turns out that the whole reconstruction procedure could be reformulated in a convenient limiting procedure, which uses only a single limiter function

$$\phi(\theta_i) = \frac{2p((p^2 - 2p\,\theta_i + 1)\ln p - (1-\theta_i)(p^2-1))}{(p^2-1)(p-1)^2} \tag{7}$$

with

$$p = p(\theta_i, q) = 2\frac{|\theta_i|^q}{1+|\theta_i|^{2q}}. \tag{8}$$

The exponent q in Eq. (8) controls the amount of the total variation of the reconstruction. It also appears as an exponent in the convergence estimate of the total variation of LDLR at jump discontinuities. We can identify the following characteristics of the limiter $\phi(\theta)$ Eq. (7):

- **i)** $\phi(1+\Delta x) = 1 + \frac{\Delta x}{3} + \mathcal{O}(\Delta x^m)$ and $\phi(-1+\Delta x) = \frac{1}{3} + \frac{\Delta x}{3} + \mathcal{O}(\Delta x^n)$ with $n, m \geq 2$
- **ii)** $\lim_{\theta\to 0}\phi(\theta) \to 0$ and $\lim_{\theta\to\pm\infty}\phi(\theta) \to 0$
- **iii)** $\lim_{q\to 0} p(\theta, q) \to 1 \quad \forall\theta \in \mathbf{R}\setminus\{0\}$ we recover $\lim_{p\to 1}\phi(\theta) \to \frac{2+\theta}{3}$, Eq. (6)

The first condition **i)** guarantees a third-order accurate resolution of local extrema, for which holds $\theta = \pm 1 + \Delta x$. It also takes care of the removable singularities at $p(\pm 1, q) = 1$. The second **ii)** ensures Eq. (7) to be local variation bounded in the presence of discontinuities. The third condition **iii)** quantifies the asymptotic behaviour of the limiter. The left plot in FIG. 1 shows the shape of the logarithmic limiter Eq. (7) for different values of the parameter q. It is obvious that the smaller q the more the reconstruction resembles the unlimited quadratic interpolation. Keeping the main features **i)**, **ii)** and **iii)** in mind, we can construct a piecewise-linear limiter function with similar properties, yet even improving its shock capturing abilities.

Without the use of a logarithmic function, we not only avoid troublesome singularities but also get better control on the reconstruction routine, thus on the total variation. The new limiter reads:

$$\hat{\phi}(\theta) = \max\left[0, \min\left[\frac{2+\theta}{3}, \max\left[-\frac{1}{2}\,\theta, \min\left(2\,\theta, \frac{2+\theta}{3}, \frac{3}{2}\right)\right]\right]\right]. \tag{9}$$

The building block of $\hat{\phi}(\theta)$ is the quadratic reconstruction of Eq. (6) for smooth data for which holds $\theta = \pm 1 + \Delta x$. The limiter is inside Harten's TVD region for $\theta \geq 0$ and recovers smooth extrema for $\theta \in [-2, -\frac{4}{5}]$ and for $\theta \in [\frac{2}{5}, \frac{5}{2}]$ to third-order accuracy. In this formulation the limiter is also contained inside Dubois's [2] extended monotonicity region. The extended monotonicity region, is indicating a domain where the resulting interpolated functions $\hat{u}^{(\mp)}_{i\pm\frac{1}{2}}$ are monotone, even though the data is not necessarily monotone. Dubois derived new monotonicity conditions for second-order limiter function which take $\theta < 0$ into account by restricting the upper bound of Harten's TVD region. The right plot in FIG. 1 shows the new limiter $\hat{\phi}$ Eq. (9) inside Dubois's extended monotonicity region matching the logarithmic limiter with $q = 1.4$.

Unfortunately in this form, the accuracy of the reconstruction still degenerates to first-order in cells with one vanishing lateral derivative $\delta_{i\pm 1/2}$. In the following we will discuss the problem of resolving smooth extrema for which $\theta \approx \pm 0$ hold with limiters. For a detailed discussion see [5]. In order to overcome this drawback we have to extend the new limiter $\hat{\phi}(\theta)$ formulation, in particular the smoothness measurement θ. We have to formulate a criterion which prohibits the limiter $\hat{\phi}(\theta)$ to pass through zero in the presence of a local extremum. For this we have introduced an asymptotic region based on the indicator

$$\eta(\delta_{i-1/2}, \delta_{i+1/2}) = \frac{\delta^2_{i-1/2} + \delta^2_{i+1/2}}{(r\,\Delta x)^2} \tag{10}$$

which is a function of the lateral derivatives $\delta_{i\pm 1/2}$, instead of θ. In addition it depends on the grid size Δx and a dimensionless constant $r \in \mathbf{R} \setminus \{0\}$. We will refer to the constant r as *radius of the asymptotic region*.

We say, that for $\eta \leq 1$ one of the lateral derivatives $\delta_{i\pm 1/2}$ is too small for θ being a good measure for smooth but steep gradients. For $\eta > 1$, $\delta_{i\pm 1/2}$ are large enough so that a limiter function based solely upon θ can be applied, e.g. $\hat{\phi}(\theta)$ Eq. (9). This definition appears at first kind of ad-hoc. But one should think of this function η exclusively as an additional indicator for smooth extrema with one vanishing lateral derivative, i.e. for $\lim_{\theta \to \pm 0} \phi(\theta) \to \pm 0$. The original reconstruction procedure

Eqs. (3) will not be changed. This function will eventually regulate the amount of total variation in the vicinity of smooth extrema or sharp gradients.

To investigate the meaning of η for continuous data with a vanishing derivative we first expand the lateral derivatives $\delta_{i\pm1/2}$ around $x_{i-1/2}$:

$$\delta_{i-1/2} = u'(x_{i-1/2})\Delta x + \frac{1}{12}u'''(x_{i-1/2})\Delta x^3 + \mathcal{O}(\Delta x^4)$$
$$\delta_{i+1/2} = u'(x_{i-1/2})\Delta x + u''(x_{i-1/2})\Delta x^2 + \frac{7}{12}u'''(x_{i-1/2})\Delta x^3 + \mathcal{O}(\Delta x^4)$$

Assuming a local extremum $u'(x_{i-1/2}) = 0$, $u''(x_{i-1/2}) \neq 0$ and cancelling higher order terms, the indicator function Eq. (10) yields

$$\eta(\delta_{i-1/2}, \delta_{i+1/2}) = \left(\frac{u''(x_{i-1/2})}{r}\right)^2 \Delta x^2 + \mathcal{O}(\Delta x^3). \tag{11}$$

Thus the function η is a measure of the second derivative, i.e. of the curvature of the data for $u'(x_{i-1/2}) \to 0$ inside a cell. Note that $\eta = \mathcal{O}(\Delta x^2)$ which is smaller than the required linear convergence of η for a third-order reconstruction. In this perspective the quadratic convergence is optimal, since one can not expect more from a three-point stencil.

We switch now to the discrete FV-setting. We consider the case of smooth extrema with one vanishing lateral derivative, i.e. $\delta_{i+1/2} \approx 0$ and $\delta_{i-1/2} \approx c\,\mathcal{O}(\Delta x^\tau)$ with $c \in \mathbf{R}$ and $\tau \in \mathbf{R}$. The asymptotic region η reads

$$\eta(0, c\,\mathcal{O}(\Delta x^\tau)) = \left(\frac{c}{r}\right)^2 \mathcal{O}(\Delta x^{2(\tau-1)}). \tag{12}$$

For $\tau \geq 1$ the lateral derivative is a smooth and bounded function and $\lim_{\Delta x \to 0} \eta = 0$ holds. Consequently we are inside the asymptotic region, i.e. the spatial reconstruction is of third-order accuracy. For $\tau < 1$ the data is discontinuous, i.e. one of the lateral derivatives is an unbounded function with a singularity in the gradient at $\Delta x = 0$. Hence we are outside the asymptotic region and full limiting is applied. If $\tau = 1$, Eq. (12) yields $\eta(0, c\,\mathcal{O}(\Delta x)) = \left(\frac{c}{r}\right)^2$. Remember we consider functions inside the asymptotic domain $\eta \leq 1$ as smooth. For $\frac{c}{r} \leq 1$ we are inside and for $\frac{c}{r} > 1$ outside the asymptotic region. Thus the parameter r plays a significant role for bounded function of $\mathcal{O}(\Delta x)$. We do not have any analytical possibility to estimate the size of the constant $|c|$. Heuristically a "large" $|c|$ might indicate discontinuous data or sharp gradients, whereas one could expect a smooth function to have a slighter curvature, i.e a "smaller" $|c|$. It is important to understand that playing with the constant r, i.e. increasing or decreasing the size of the asymptotic domain clearly affects the amount of introduced variation. Thus we switch to full limiting already on a coarse grid in the presence of a jump discontinuity. Remember a scheme based upon classical TVD limiters would result in a first-order reconstruction of the cell interface values independent of the parameters c or τ. Finally our new third-order limiter function reads:

$$\phi^{\mathcal{O}(3)}(\delta_{i-1/2}, \delta_{i+1/2}) = \begin{cases} \frac{2+\theta}{3} & \text{if } \eta \leq 1-\epsilon \\ \hat{\phi} & \text{if } \eta \geq 1+\epsilon \\ \frac{1}{2}\left(\left(1-\frac{\eta-1}{\epsilon}\right)\frac{2+\theta}{3} + \left(1+\frac{\eta-1}{\epsilon}\right)\hat{\phi}\right) & \text{else} \end{cases} \tag{13}$$

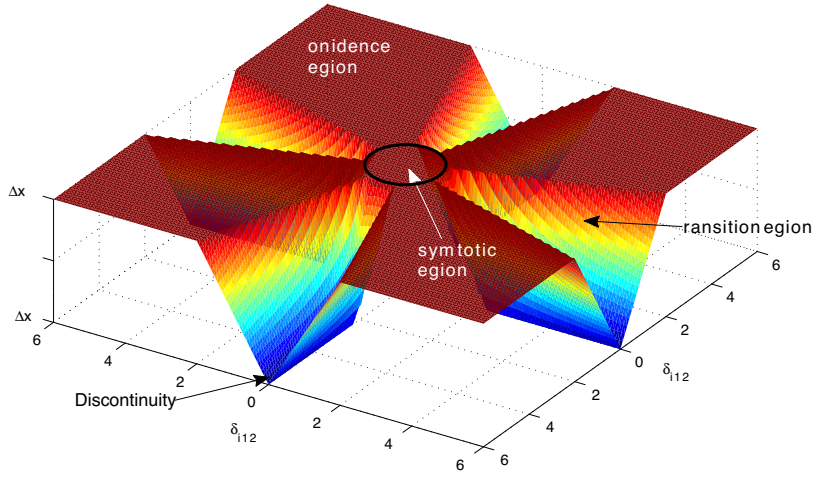

FIG. 2. *Sketch of new reconstruction routine including the asymptotic region for smooth extrema with one vanishing lateral derivative* $\delta_{i\pm1/2}$. *Red color indicates third order recovery.*

with ϵ being a small positive number, which is about the size of the particular machine precision and ensures Lipschitz continuity for $\phi^{\mathcal{O}(3)}$ Eq. (13). Note that in the proposed limiter, the problem of accurately recovering smooth extrema with one vanishing lateral derivative and simultaneously reconstructing sharp gradients is rigorously decoupled. Consequently, in the presence of a discontinuity, i.e. $\tau = -1$ we get $\eta(0, c\,\mathcal{O}(\Delta x^{-1})) = \left(\frac{c}{r}\right)^2 \mathcal{O}(\Delta x^{-4})$, hence fourth-order convergence towards infinity. The new limiter yields $\phi^{\mathcal{O}(3)} \to \hat{\phi}(0) = 0$ with $\mathcal{O}(\Delta x^4)$. Because of the decoupling, the character of the limiter $\hat{\phi}(\theta)$ is not changed. It remains a monotone homogenous function of degree one, i.e. $\hat{\phi}(\lambda\,\theta) = \lambda\,\hat{\phi}(\theta), \quad \forall\lambda \in \mathbf{R}$ and $\min(\delta_{i-1/2}, \delta_{i+1/2}) \leq \hat{\phi}(\theta) \leq \max(\delta_{i-1/2}, \delta_{i+1/2})$. These are the main ingredients for a reconstruction to be TVD.

FIG. 2 points out the characteristic properties of the final limiter $\phi^{\mathcal{O}(3)}$ Eq. (13). It is, for simplicity, more a sketch rather than an actual plot of the function $\phi^{\mathcal{O}(3)}$. This way we can geometrically clarify the asymptotic region η, the confidence region and the transition domain. In the first two regions the interface values are reconstructed to full third-order of accuracy, since we are "confident" that the input data is smooth, i.e. $\tau > 1$ and $\frac{c}{r} \leq 1$ in Eq. (12). Whereas in the transition region the discretized input data is discontinuous. In other words $\tau < 1$ or $\frac{c}{r} \gg 1$ in Eq. (12) and consequently the data has to be fully limited. The lower limit $(1 - \epsilon)$ and upper limit $(1 + \epsilon)$, i.e. the thickness of the dark circle around the asymptotic region ensure Lipschitz continuity of the limiter $\phi^{\mathcal{O}(3)}$. Therefor the numerical flux function $\mathcal{F}$ in Eq. (2) is also Lipschitz continuous away from the asymptotic domain. Cuts along constant $\delta_{i-1/2}$ correspond to the limiter function FIG. 1, right plot.

4. Numerical Experiments. We reduce our numerical test cases solely to the linear advection equation. A more ellaborate collection of test cases including Euler

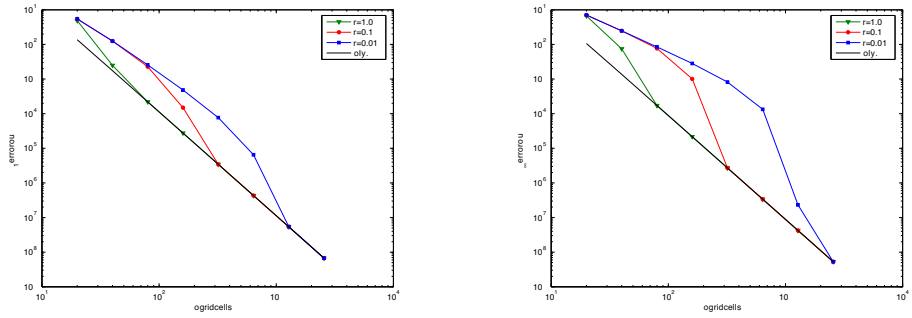

FIG. 3. *Log-log-plots:* $u_0(x) = \sin(\pi\, x), t = 1, \nu = 0.9$.

equations in 1D and 2D can be found in [5]. The 1D linear advection equation reads

$$u_t = -u_x, \quad u(t=0,x) = u_0(x). \tag{14}$$

The boundaries are set to be periodic on the domain $x \in [-1,1]$ for all numerical experiment. The purpose is to examine the effects of the asymptotic region, in particular of its the radius r on the accuracy of the reconstruction quality. We use the explicit third-order TVD Runge-Kutta (RK3rd) method of Gottlieb and Shu [3] in combination with $\phi^{\mathcal{O}(3)}$ Eq. (13). Second-order accurate limiter function are combined with the Heun time marching scheme.

Example 1: We solve Eq. (14) with $u_0(x) = \sin(\pi\, x)$. FIG. 3 shows the computed L_1- and L_∞-errors obtained at $t = 1$ with Courant number $\nu = 0.9$. We compare the accuracy to the pure unlimited quadratic interpolation Eq. (6). This gives a clear impression when –in terms of spatial resolution Δx and radius r– the optimal error is reached. The formal third-order convergence rate is already achieved with only 40 cells. Yet it is obvious that the designated accuracy is only reached with more cells, especially for a small asymptotic region $r \leq 0.01$.

Example 2: In FIG. 4 we clarify the effect of the asymptotic region for discontinuous data. We conduct numerical experiment with a square- and sin-wave using 200 grid-cells. Choosing a small radius $r \leq 0.01$, the limiter needs a sufficient resolution, to be able to distinguish between a discretized smooth extremum or a shallow gradient. We can also observe that even for a large asymptotic region, essentially no limiting, the method does not become unstable, unlike an unlimited second-order TVD-method. The over- and under-shoots remain localized and do not grow with time, which is an effect of the rather diffusive character of third-order methods. Note that the two profiles are advected ten times ($t = 20$).

Example 3: To test the shock capturing properties and the shape preserving quality of the proposed limiter, we choose initial conditions with discontinuities.The test case consists of a tight combination of four waves, namely a smooth but narrow Gaussian peak, a square wave, a triangle wave and a half ellipse. The triangle has a smooth transition at its base. The initial profile is advected until $t = 20$. In Fig. 5 we compare our new limiter function $\phi^{\mathcal{O}(3)}$ (LimO3) with third-order ENO method (ENO3) and with LDLR. ENO3 is essentially not local since it uses a five point stencil to choose between the "smoothest" reconstruction for the interface values. All

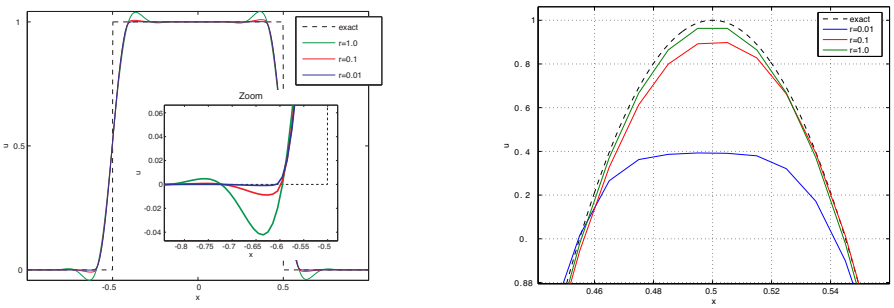

FIG. 4. *Left: Square wave. Right: Sin-wave,* $t = 20, \nu = 0.8$.

schemes use the same explicit third-order Runge-Kutta method for time integration.

Especially in contrast to the classical TVD-MUSCL scheme (see FIG. 5 bottom), the new method gives a good approximation of the exact profile. Typical drawbacks of second-order TVD limiter, such as smearing and squaring of linear waves are completely avoided. The results are perfectly symmetric and corners a very well resolved. The symmetry of the results is due to the fact, that near $\theta = 1$ we recover a smooth function of second degree. Whereas second-order TVD limiters, such as super-bee or minmod, are only Lipschitz continuous near $\theta = 1$. This drawback enhances the probability, that the wrong choice of slopes is used for the one-sided approximation. Furthermore third-order algorithms exhibits a rather dissipative character, whereas second-order accurate schemes a rather dispersive. Therefor even smooth second-order accurate limiters, such as van Leer, MCD (see e.g. [7]) do not give symmetric profiles.

Both LimO3 and LDLR are essentially of the same quality, yet LimO3 has a higher Gaussian peak and produces less overshoots for the half ellipse. Whereas ENO3 is not able to distinguish between the different waves and always produces sinusoidal-like wave patterns. All three method produce negative values, yet for LimO3 they are of a smaller magnitude. Remember the asymptotic region scales, in the presence of jump discontinuities, with $\mathcal{O}(\Delta x^4)$.

Example 4: In order to examine the TVB properties of the proposed scheme, we solve Burger's equation

$$u_t = -\left(\frac{u^2}{2}\right)_x, \quad u_0(x) = 1 + \frac{1}{2}\sin(\pi(x-1)) \tag{15}$$

on a periodic domain $x \in [-1, 1]$ under CFL condition $\nu = 0.9$. FIG. 6 (left) shows the numerical behavior of the total variation for Burger's equation and the LimO3 approximation at $t = 2.0$. We calculate for both equations the total variation for a grid function $\bar{u}$: $TV(\bar{u}^n) \equiv \sum_{i=1}^{N} |\bar{u}_{i+1}^n - \bar{u}_i^n|$. We observe that the calculated variation is bounded by the initial variation $TV(\bar{u}^0)$ and gradually decreases with time as a jump discontinuity forms at $t \approx 1.0$. In contrast to LDLR, the accuracy of the solution with 40 cells is significantly better (see [1]) and the evolving smooth profile for $t \in [0, 0.8]$ is recovered accurately. Note that for all three resolutions the value

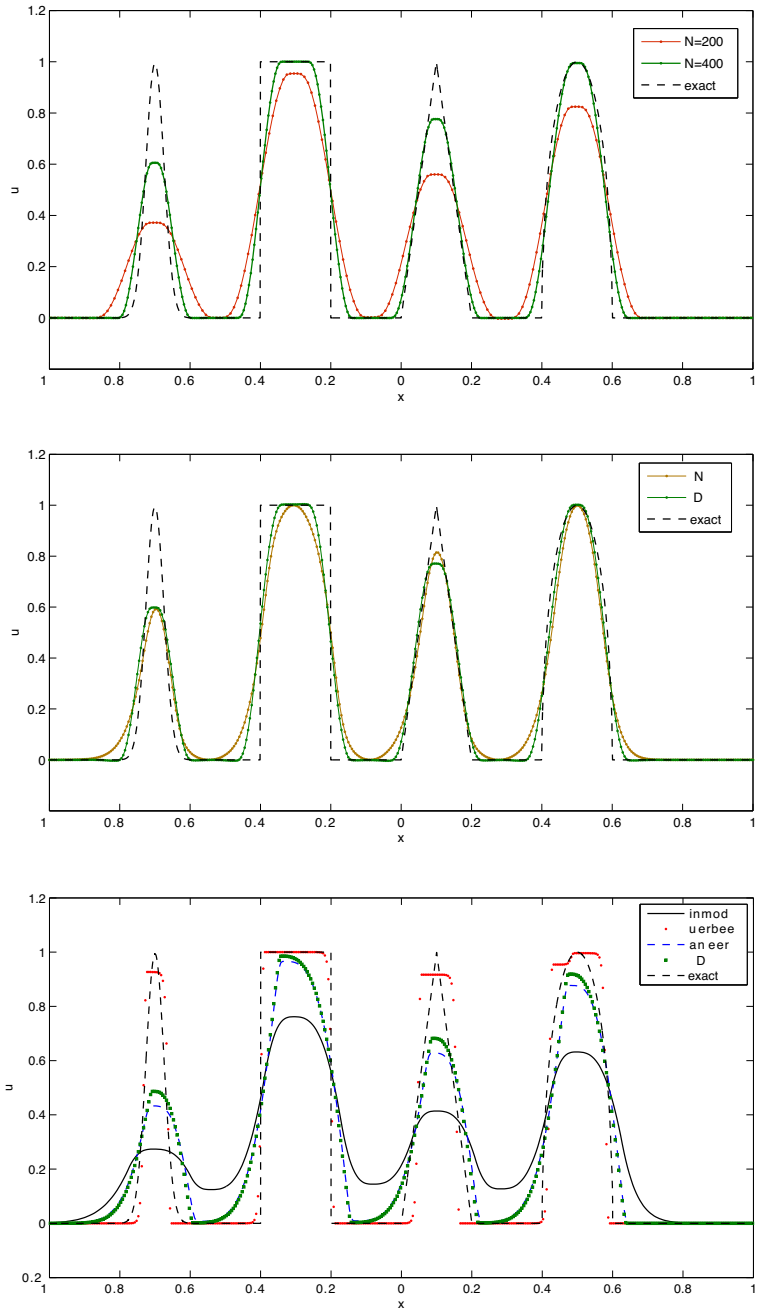

FIG. 5. *Advection of discontinuities with* $\nu = 0.8$ *until* $t = 20$. *Top profile: Proposed method LimO3 on 200 and 400 cells with the radius* $r = 0.01$. *Middle profile: LDLR and ENO3 taken from [1] on 400 cells with* $\nu = 0.6$. *Bottom profile: Second-order accurate limiters combined with the Heun time integrator on 400 cells with* $\nu = 0.8$.

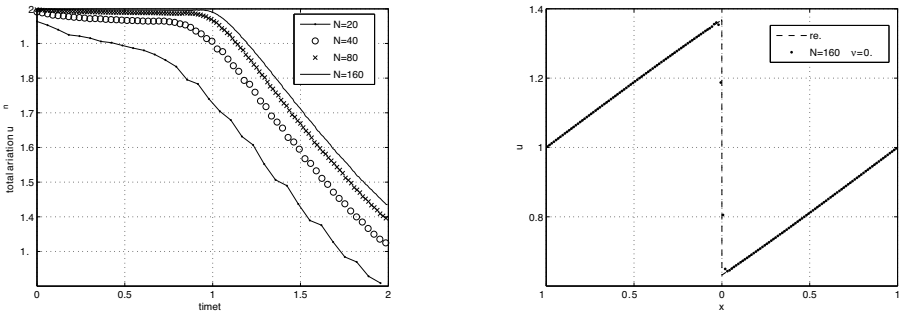

FIG. 6. *Total variation of Burger's equation (left) and LimO3 approximation with* $\nu = 0.9$ *and* $r = 0.1$ *at* $t = 2.0$

of total variation before the shock forms is always larger than of LDLR. Hence the smooth profile is resolved more accurately with few computational cells. This could even be improved with a larger asymptotic region, yet also leading to larger, but bounded spurious oscillations shortly before the jump discontinuity forms. However once the discontinuity clearly appears the limiter yields $\phi^{\mathcal{O}(3)} \longrightarrow \hat{\phi}(0) = 0$ and the oscillations completely disappear.

5. Conclusions. We have derived and analyzed a new third-order limiter for the numerical solution of hyperbolic conservation laws. In contrast to classical second-order TVD-limiters, the proposed limiter function maintains its formal accuracy at local extrema. It has very good shape-preserving properties and known limiter effects, such as smearing and squaring do not appear. The proposed limiter employs a local piecewise parabolic reconstruction for smooth data and preserves accuracy within the asymptotic region. Numerical experiments indicate the superiority of the proposed limiter over classical second-order TVD limiters. The new scheme also compares favorably with third-order methods such as LDLR and ENO3. It is computationally more economical than ENO scheme, because costly optimal stencil searches and memory storage are avoided.

REFERENCES

[1] R. ARTEBRANT AND H. J. SCHROLL, *Limiter-free third order logarithmic reconstruction*, SIAM, J. Sci. Comput., 28, 359–381, 2006.

[2] F. DUBOIS, *Nonlinear Interpolation and Total Variation Diminishing Schemes.* Rapport de recherche Aerospatiale Escape et Defense, ST/S 46 195, 1993.

[3] S. GOTTLIEB AND C.-W. SHU, *Total Variation Diminishing Runge-Kutta Schemes.* Math. Comput., 67, pp. 73–85, 1983.

[4] A. HARTEN, *High resolution schemes for hyperbolic conservation laws.* J. Comput. Phys., 59, pp. 357–393, 1983.

[5] M. ČADA AND M. TORRILHON, *Compact third order limiter functions for Finite-Volume-Methods.* ETH SAM-Report 12, 2008.

[6] J. C. SWEBY, *High resolution schemes using flux limiters for hyperbolic conservation laws.* SIAM J. Num. Anal., 21, pp. 995–1011, 1984.

[7] R. J. LEVEQUE, *Finite Volume Methods for Hyperbolic Problems.*, Cambridge Texts in Applied Mathematics, 2003.